Wear 319 (2014) 200–210

Contents lists available at ScienceDirect

Wear

journal homepage: www.elsevier.com/locate/wear

Effects of microstructures on the sliding behavior of hot-pressed CoCrMo alloys

Yan Chen [a], Yunping Li [b,*], Shingo Kurosu [b], Kenta Yamanaka [b], Ning Tang [b], Akihiko Chiba [b]

[a] Tohoku University, Department of Material Science and Engineering, Sendai 980-8579, Japan
[b] Institute for Material Research, Sendai 980-8577, Japan

ARTICLE INFO

Article history:
Received 3 March 2014
Received in revised form
17 July 2014
Accepted 24 July 2014
Available online 13 August 2014

Keywords:
Lamellar precipitate
ε-H.C.P. phase
Sliding wear
CoCrMoC alloy

ABSTRACT

Cobalt–chromium–molybdenum (CoCrMo) alloys are widely applied as wear-resistant material. This article aims to illustrate the influence of phase constitution and precipitate morphology on the wear behavior of hot-pressed high carbon alloys. Wear behavior of two kinds of CoCrMo alloys, HP (hot-pressed) and HPA (hot-pressed + annealing) with various microstructure, hardness and surface topography were evaluated in detail. The ε phase dominant HP alloy with homogenous lamellar precipitates demonstrates higher hardness, consequently lower coefficient of friction and prominent wear resistance with mild sliding wear. In contrary, the γ phase dominant HPA alloy with carbide-free grains was characterized by abrasive wear of micro grooves. The matrix hardness strengthened by ε phase is more significant to affect wear behavior than precipitate hardening. Homogenous lamellar precipitates have a stand-out effect to block abrasion and accumulate tribochemical products.

1. Introduction

The cobalt–chromium–molybdenum (CoCrMo) alloys, owing to their mechanical properties, high wear and corrosion resistance, have wide applications as wear-resistant components for such as metal-on-metal (MOM) hip replacement, dental devices as well as other structural components [1,2]. Mechanical properties of CoCrMo alloys, dependent on their microstructures, could be enhanced by solid-solution and/or surface hardening [3,4], manufacturing process and subsequent heat treatments [5,6], and precipitation (carbides, nitrides, etc.) hardening [7].

Previous studies have indicated that microstructural control can significantly improve the mechanical properties of CoCrMo alloys [8]. To date, casting and forging are the most commonly used manufacturing process. The former is the most conventional method but is limited in enhancing the mechanical properties [9]; whereas the latter, via forging or working on the cast ingot under hot or cold environment, has been proved to be a more effective method to improve the properties [10]. In addition, recent researches also indicate that hot pressing (HP) on alloy powder has been used as an emerging processing method to control microstructures of the materials in the field of industrial engineering [8,11–13]. Compared to the casting and forging processing mentioned above, the HP process can obtain microstructures with homogeneous chemical composition, high density, free of pores and hard precipitates, thereby the enhanced mechanical and electrochemical properties [11–13].

Increasing carbon and nitrogen content was designed to obtain CoCrMo alloys with enhanced mechanical properties and wear response, which has been revealed by previous studies. However, microstructures generated under various processes or heat treatments showed different responses to expectation, and if the matrix phase constitution and the type, morphology, size, distribution of the carbide and nitride precipitates are improperly controlled, they would accordingly result in loss of the desired properties or potential material failure [3] [14–20]. To date, few researches have been focused on the tribological properties of the HP CoCrMo alloys with various microstructures. The aim of this study was to elucidate the influence of the microstructure factors on the sliding behaviors of the high-carbon (HC) CoCrMo alloys manufactured by HP process for wear-resistant application.

2. Experimental procedure

2.1. Materials and processing

The alloy was produced by hot pressing using high carbon (HC) spherical CoCrMo powders (Sanyo special steel, Japan), and the chemical composition of the powder is listed in Table 1. The schematic

* Corresponding author. Tel.: +8122 215 2452; fax: +8122 215 2116.
E-mail addresses: chenyan@imr.tohoku.ac.jp (Y. Chen), lyping@imr.tohoku.ac.jp (Y. Li), kurosu@imr.tohoku.ac.jp (S. Kurosu), k_yamanaka@imr.tohoku.ac.jp (K. Yamanaka), ningtang@imr.tohoku.ac.jp (N. Tang), a.chiba@imr.tohoku.ac.jp (A. Chiba).

http://dx.doi.org/10.1016/j.wear.2014.07.022
0043-1648/

representation of the hot pressing is shown in Fig. 1. Before the processing, the CoCrMo powders were dried to remove the humidity, and then induction-melted under an argon gas atmosphere. After that they were classified with a sifter to obtain particles less than ~100 μm and encapsulated into a ⌀ 150 mm billet, ~7 Pa. The billet was heated up to 1473 K with a heating rate of 0.167 K/s, and kept at 1473 K for 1.26×10^4 s. The hot pressing was performed under vacuum and a constant pressure of 594 MPa to prevent pores generation. Then the ingot was cooled from ~1100 K to 293 K for 48 h in the furnace.

To obtain CoCrMo alloys with different microstructures, the hot-pressed material underwent further annealing at 1373 K for 600 s, using a muffle furnace (Fo200, YAMATO), followed by a water quenching. A temperature of 1373 K is the temperature for γ-F.C.C and ε-H.C.P. phase transition, as we indicated in the phase diagram (Fig. 2), and a 600 s annealing above the phase transition temperature, the reverse transformation would be sufficient to get a γ-F.C.C matrix and fine grains [15]. For convenience, the samples obtained from hot pressing process and that with annealing are hereafter designated as HP and HPA, respectively.

2.2. Microstructure characterization

Pins and discs were machined into dimensions of ⌀6 mm × 20 mm and ⌀30 mm × 5 mm, respectively. The spherical contact ends of the pins (*SR* 2.4 mm) were ground with emery paper of up to # 6000 grit and polished with a silica suspension. The discs were prepared with a sequence of abrading with #180–1200 grit emery papers, 30-min polishing with alumina and silica suspensions, and finally electro-polishing in an electrolyte (methanol: sulfuric acid = 9:1) at 6 V, room temperature for 5 s. The microstructure of disc surface was observed by performing scanning electron microscopy (SEM, Hitachi S3400N) and transmission electron microscope (TEM, JEM-2000EX II). The phase constitution of the matrix was identified by performing X-ray diffraction (XRD, Philips X' Pert) measurements with Cu Kα radiation over $40° < 2\theta < 55°$, focused on three locations on each specimen.

Table 1
Chemical composition of HC CoCrMo powders (wt%).

Co	Cr	Mo	C	Si	Mn	W	N
Bal.	26.9	6.1	0.27	0.63	0.59	0.02	0.17

2.3. Pin-on-disc test

The pin-on-disc test was conducted using a RHSCA FRP-2000 tribometer and the experimental conditions are same as our previous

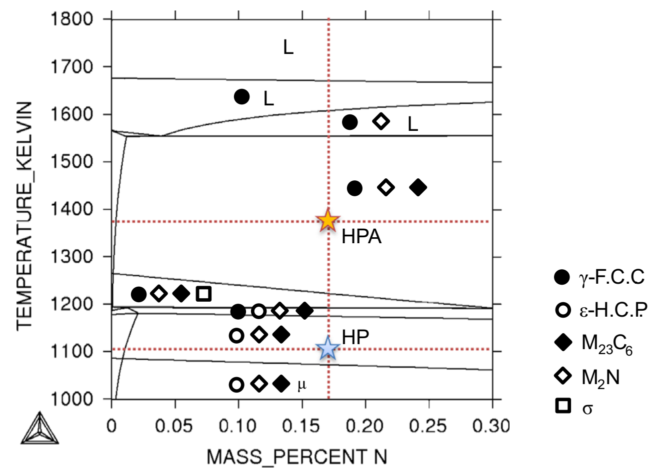

Fig. 2. Phase diagram calculated using Thermo-Calc software for Co–27Cr–6Mo–N (wt%) systems, in which HP and HPA show single ε-H.C.P. and γ-F.C.C. matrix, respectively.

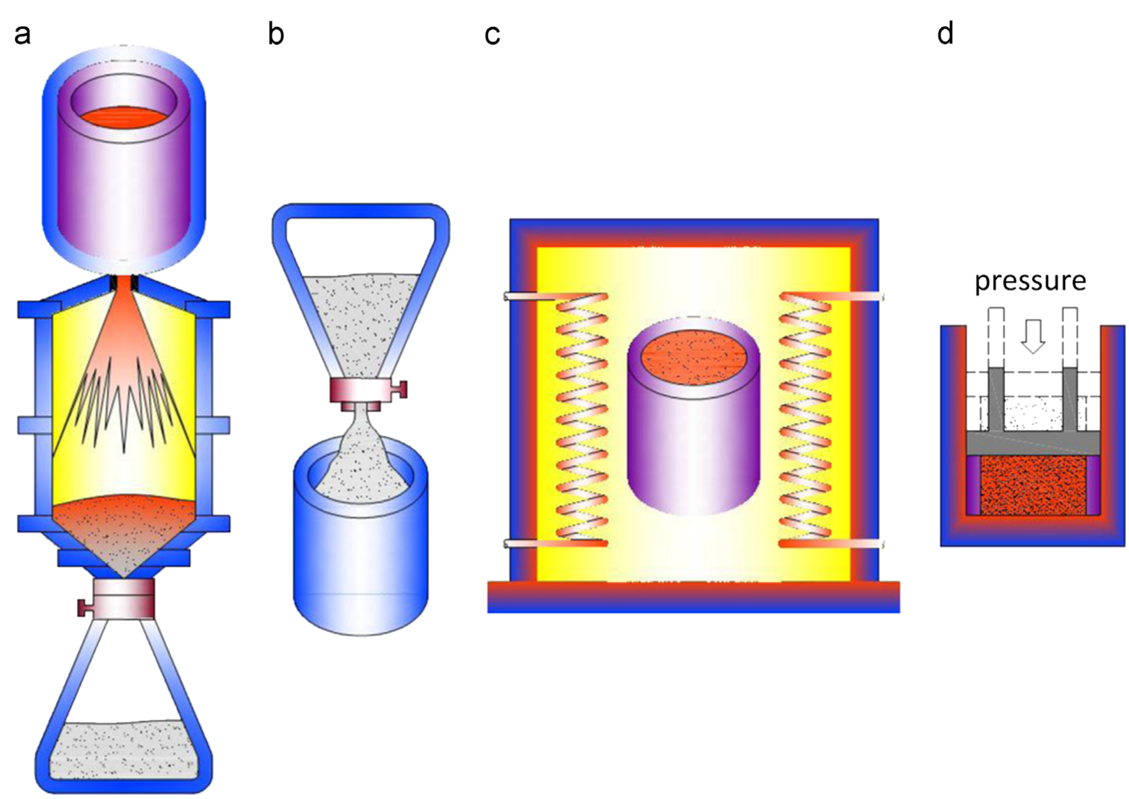

Fig. 1. Schematic representation of the alloy manufacturing process: (a) vacuum induction melting and inert gas atomizing, (b) classifying and encapsulating; (c) billet heating; (d) hot pressing.

study [22]. The pin was mounted with a 9.8 N load representing a harsh contact (initial contact pressure: 1.69 GPa), and tested against a disc rotating at 20 mm/s (24 rpm). In order to evaluate the wear behavior of the present alloys under a more severe condition than the generally used protein-containing condition for artificial hip joint, the wear tests were conducted under Hanks' lubricated environment. Under this protein-free condition, the samples are subjected to a heavier wear due to the lower lubricating effect of Hanks solution. The test was performed over a continuous period of 60.48 ks for a total sliding distance of ~12.1 km. All tests were repeated for three times.

The worn specimens were cleaned ultrasonically in distilled water and ethanol, and then dried for weight loss measurement using a direct-reading balance (Shimadzu AUW 320). The wear factor was calculated according to [23]:

$$\omega_s = M_{loss}/(w \cdot s \cdot \rho) \quad (1)$$

where M_{loss} is weight loss, w is the normal load, s is the sliding distance, and ρ is the density of the specimen.

The wear scars were analyzed using XRD, SEM and laser microscope (LM, Keyence KV-x200 series). Micro hardness was measured using a Vickers hardness tester (Shimazu, HMV) with the Vickers indentation method (ASTM E92)[24]. The roughness of as-polished and worn surfaces were evaluated with a stylus profilometer (Surfcorder DSF 500). The hardness and roughness were taken 10 and 6 measurements, respectively.

3. Results

3.1. Material characterization

Fig. 2 shows the phase diagram for Co–27Cr–6Mo–0.27C (wt%) alloys, using Thermo-Calc 5.0 TCW (Thermo-Calc Software, Stockholm, Sweden) with a Ni-based alloy database, including the type and quantity of the phases in thermodynamic equilibrium. The dominating phases of the HP and HPA matrices (0.17% N) are the ε-H.C.P and γ-F.C.C. phase, respectively, with possible phases of M23C6 (M=Cr, Mo) carbides and M_2N phase nitrides existing as precipitates.

Rough phase constitution of the matrix estimation was also estimated by XRD as shown in Fig. 3, and they were observed to resemble with the calculation results.

SEM micrographs in Fig. 4 show the microstructures of (a)–(c) HP and (d)–(f) HPA alloys, which comprise plenty of lamellar precipitates precipitating along the grain boundaries and inside the grains (average grain size: ~50 μm). No obvious pores were observed in the alloys. The results indicate that for HP, an overall distribution of the hybrid coarse platelet-like and fine acicular lamellae (bright) was observed inlaying separately in the grains (dark); for HPA, platelet-like structure (bright) remain exist, whereas most fine acicular lamellae dissolved in the matrix (dark) as a result of annealing treatment. The grains absent of the fine acicular lamellae indicate that these precipitates were dissolved and distribute in nanosize throughout the matrix [21].

Qualitative analysis on the microstructures of HP and HPA was conducted by TEM. Fig. 5 shows the matrices and their diffraction patterns in (a) (a′) for HP, and (b) (b′) for HPA. The results were same as that of the calculation and XRD (see Figs. 2 and 3), indicating that the HP and HPA matrices are ε-H.C.P and γ-F.C.C., respectively. The precipitates and their diffraction patterns in Fig. 6 (a), (b) and (c) in HP and HPA. The platelet-like precipitates are verified to be cubic $M_{23}C_6$ (a)(c), whereas the fine acicular ones were hexagonal M_2N(b).

The average true-spacing between the lamellae, $\bar{L}_0$, was measured by involving a circular test grid (∅: d_c), the number n of

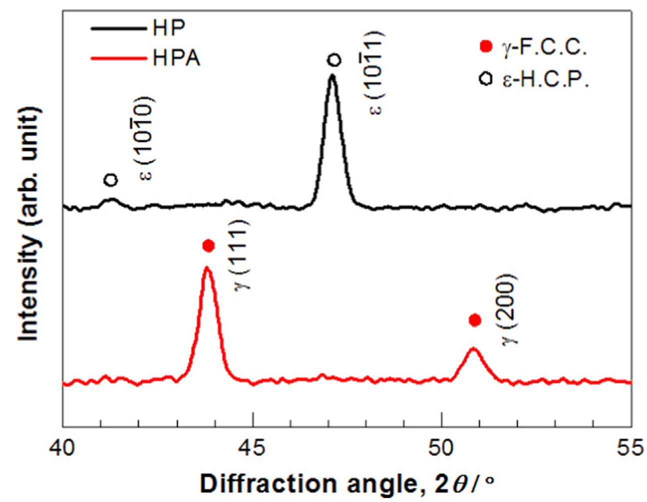

Fig. 3. X-ray profiles of as-polished HP and HPA discs, indicating they are ε-H.C.P and γ-F.C.C. matrix, respectively (three measurements for each material).

intersections with lamellae yields the true spacing [25]:

$$\bar{L}_0 = \frac{\pi d_c}{2nM}$$

in which M is the magnification. Three random locations were measured on the platelet-like $M_{23}C_6$ and acicular M_2N, to find that $\bar{L}_0$ are ~0.58 μm and ~0.35 μm, respectively.

3.2. Wear behavior

3.2.1. Coefficient of friction

Fig. 7 (a) and (b) shows the dynamic and mean coefficients of friction of HP and HPA alloys under constant 9.8 N loads. The dynamic coefficient of friction of HP had a steep slope for the first 0.1 km, however, that of HPA had a slope lasted for the first 1 km, for their respective "run-in" stages. Then both of the dynamic coefficients of friction increased gently, which indicates a subsequent "stable" stage [26,27]. The stable coefficients of friction at this stage were observed to be 0.33 and 0.52 for HP and HPA, respectively, and the Student's t-test (assuming unequal variances; two-tail, $P<0.05$) indicated that they exhibited significantly differences. The HP exhibited extremely low coefficient of friction with less "noisy," which was considered to endure less tangential friction and smoother contact than the HPA during the wear test.

3.2.2. Volume loss

Fig. 8 shows the volume losses (mm^3) of HP and HPA alloys after 1.2 km sliding. It illustrates that the HP used in the present study exhibited much higher wear resistance compared to the HPA. Wear factors ($\times 10^{-7}$ mm^3/N m) for the alloys, according to Eq. (1), were calculated to be 12.6 and 25.5 for HP and HPA, respectively, which agree with the respective volume losses. The pins experienced lower wear than the corresponding discs for both alloys. According to Student's t-test (assuming unequal variances; two-tail, $P<0.05$), no significant difference was observed between the volume wear of the HP and HPA pins; but significant differences were found between that of the discs. We assume that the asymmetry form of the pin-on-disc apparatus would be the possible reason for the asymmetry wear of pin and disc, and both the pins with continuous contact experience similar higher temperature and wear rate.

3.2.3. Surface topography

The SEM micrographs on the wear tracks on HP and HPA discs are shown in Fig. 9 (a) (b) and (c) (d), respectively, in which the

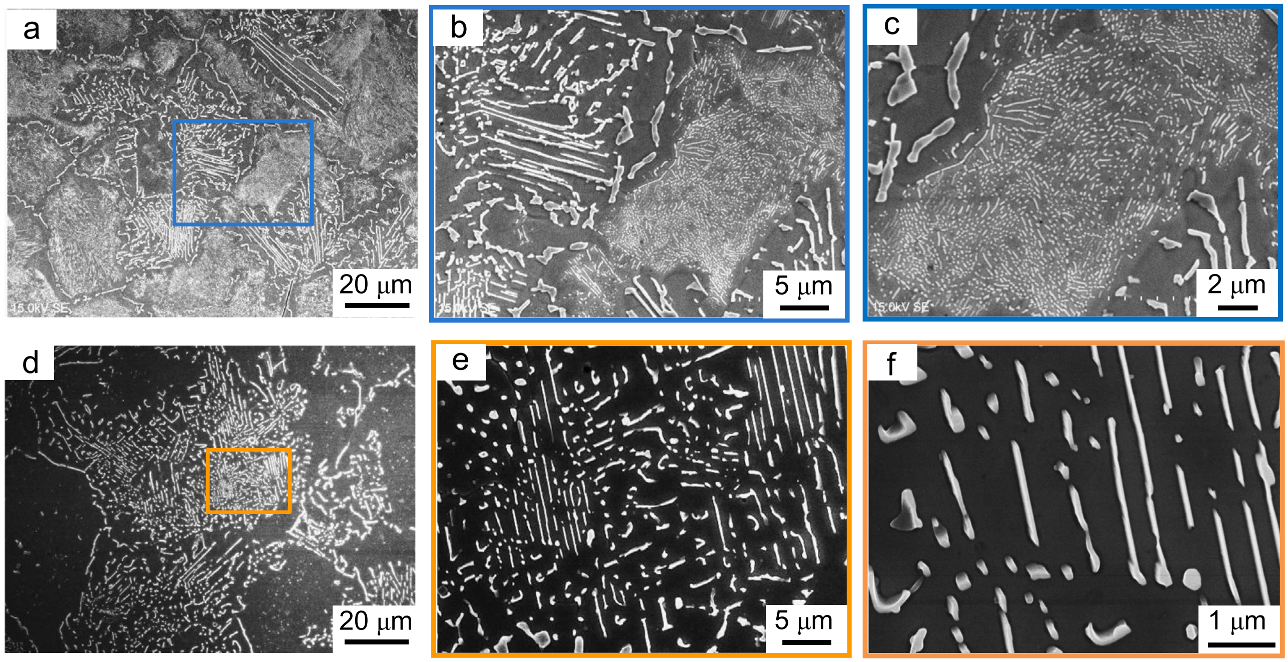

Fig. 4. SEM micrographs showing the microstructures in which lamellar eutectic precipitates with different fineness: (a)–(c) hybrid platelet-like and acicular structure (bright) in separate HP grains (dark); (d)–(f) platelet-like structure (bright) in partial γ-F.C.C. HPA grains (dark).

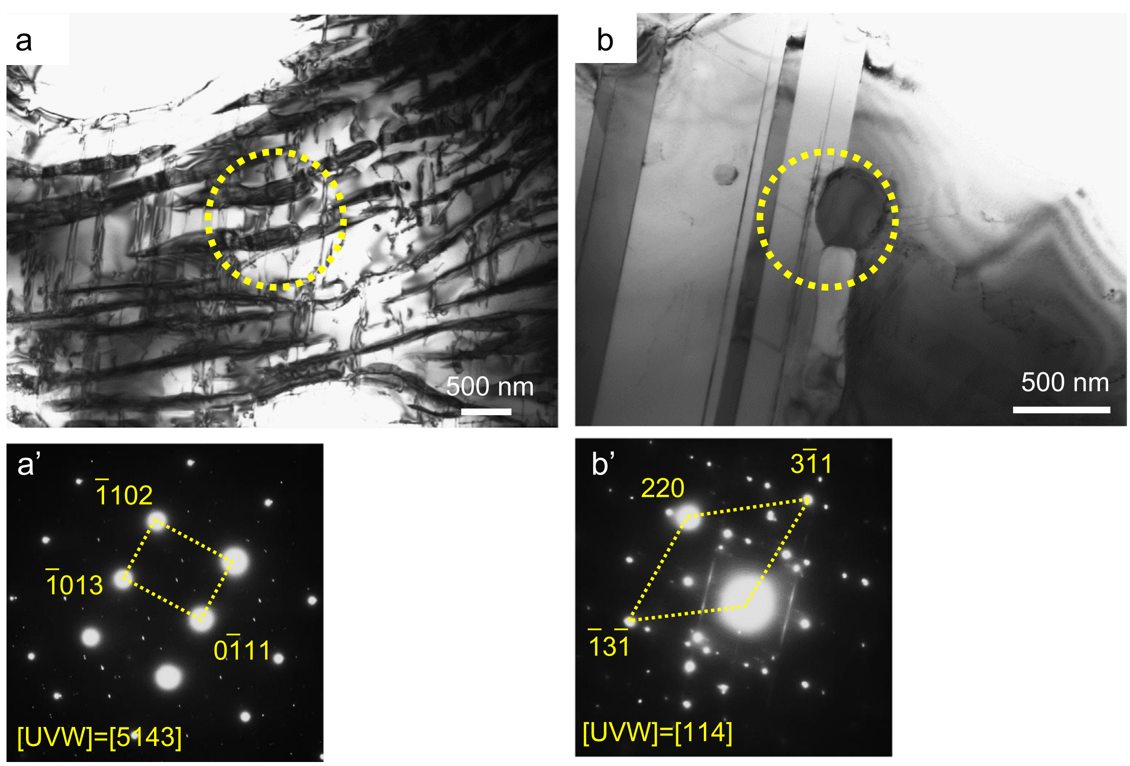

Fig. 5. TEM micrographs for qualitative analysis of matrices, indicating that (a) (a′) ε-H.C.P HP and (b) (b′) γ-F.C.C. HPA.

sliding directions of the pins are indicated by white arrows. The images of (a) and (c) depict some stripe traces in the track, where harsh contact occurs; flaky deposition (dark strips) were observed covering on the surfaces nearby, where mild contact occurs. It is remarkable that obvious groove was observed in the HPA wear track (bright long line in (c)), indicating that the material may have endured serious plastic deformation. The detailed topography in (d) also shows that compared with large amount of plastic scuffing, the precipitates are less obvious. However, scarce abrasion of similar scuffing but plenty of lamellae with obvious adhesion was found residual on the worn HP surface.

Fig. 10 shows the SEM micrographs of the worn HP ((a) (b)) and HPA ((c)(d)) surface topographies of the pins. Similar to the wear tracks on the discs, stripe wear zones concentrated in the center of the worn circular zones in Fig. 10(a) and (c) where maximum contact pressures occur, which were observed stretching along sliding directions indicated by white arrows for the both alloys. Compacted deposition layer were observed on the boundary

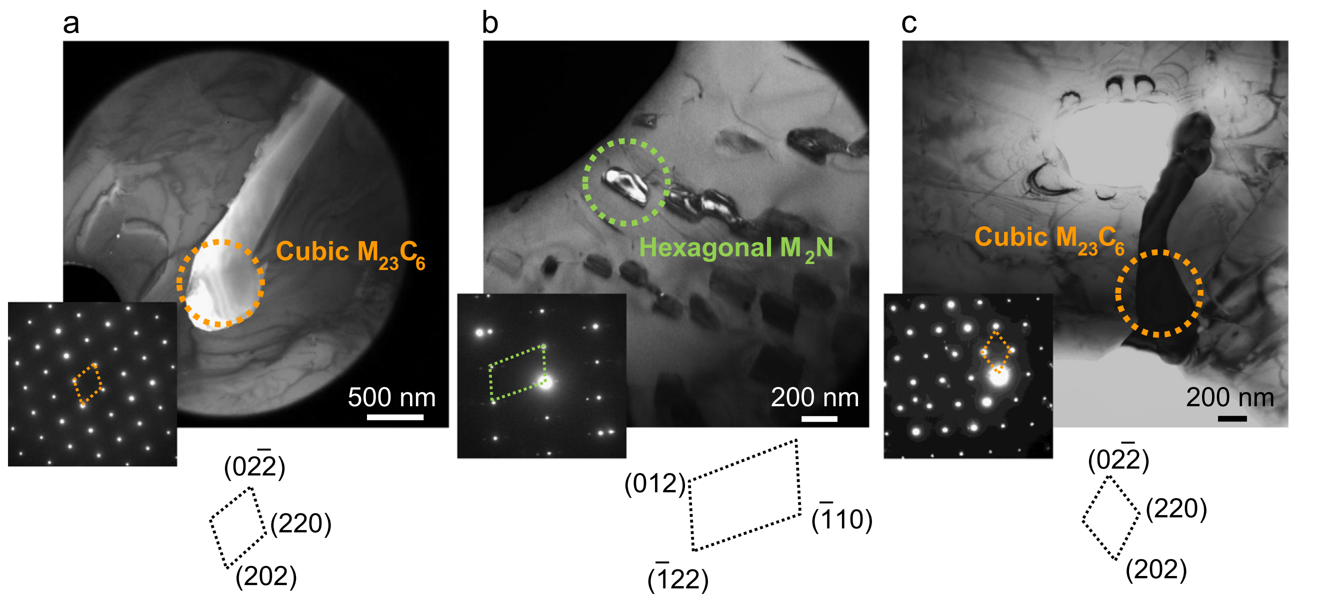

Fig. 6. TEM micrographs for qualitative analysis of precipitates: dark field images of (a) platelet-like cubic $M_{23}C_6$ and (b) acicular hexagonal M_2N in ε-H.C.P HP, bright field image of (c) platelet-like cubic $M_{23}C_6$ in γ-F.C.C. HPA.

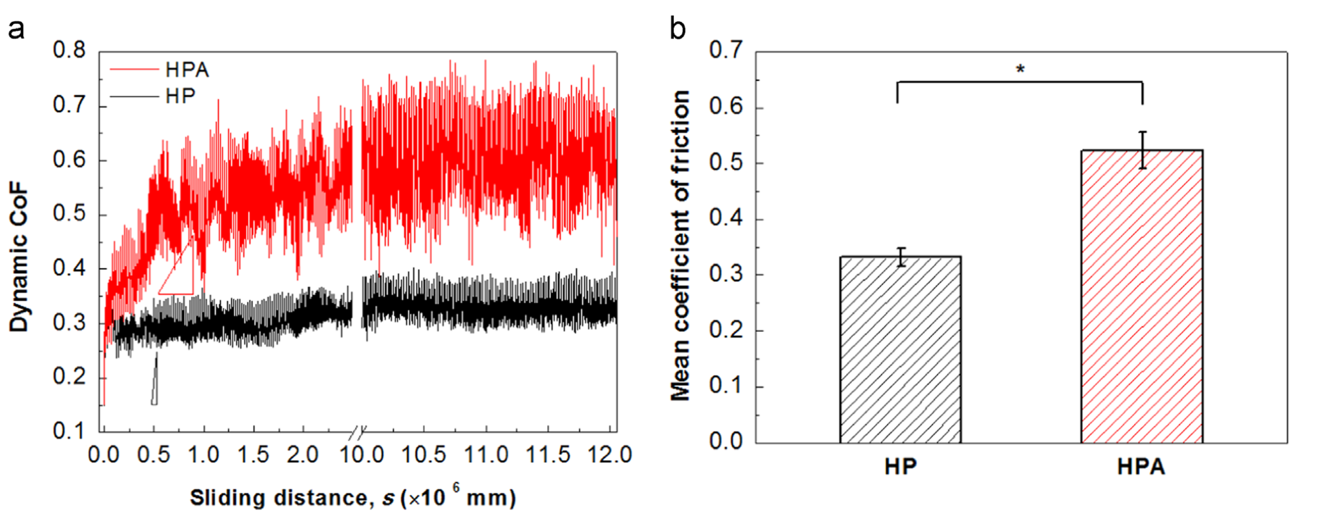

Fig. 7. (a) Dynamic and (b) mean coefficients of friction for HP and HPA alloys under constant 9.8 N loads in Hanks' solution, in which HP endured extremely lower coefficient of friction with less "noisy." Asterisks denote significant differences for mean coefficients of friction of HP and HPA alloys according to the Student's *t*-test with $P<0.05$, and error bars denote the mean ± standard deviation.

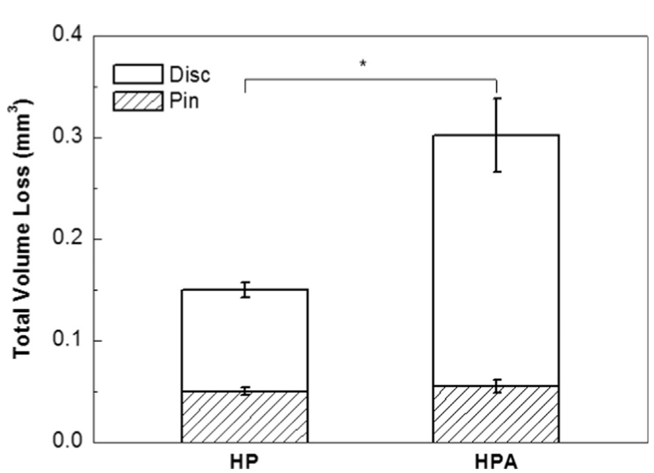

Fig. 8. Total volume loss of the HP and HPA alloys after wear tests with their error bars (standard deviation), in which HP exhibits excellent wear resistance.

between the worn and unworn HP zones, however, few depositions were found on that of the HPA pin. Concentrations of abrasive scuffing of HP and HPA were observed under higher magnification in Fig. 10(b) and (d), respectively. The worn HP surface demonstrates more obvious adhesion scattered between the scratches than HPA surface.

The 3D micrographs of the macro worn surface topography are shown in Fig. 11, for (a) HP, (b) HPA discs, and (c) HP, (d) HPA pins, respectively. Abrasive wear characterized by inhomogeneous deformable groove zone was observed for the HPA, whereas homogeneous sliding wear with obvious deposition layers for the HP.

A backscattered electron (BSE) image in Fig. 12(a) indicates that more deposition layers were observed to delaminate on the HP surface, under or between which lamellae precipitates exist. The X-ray mappings (Fig. 12(b)–(d)) show that the accumulation of depositions were enriched with calcium, oxygen and phosphorous; thus they are conjectured as kind of Ca-PO4 compound by

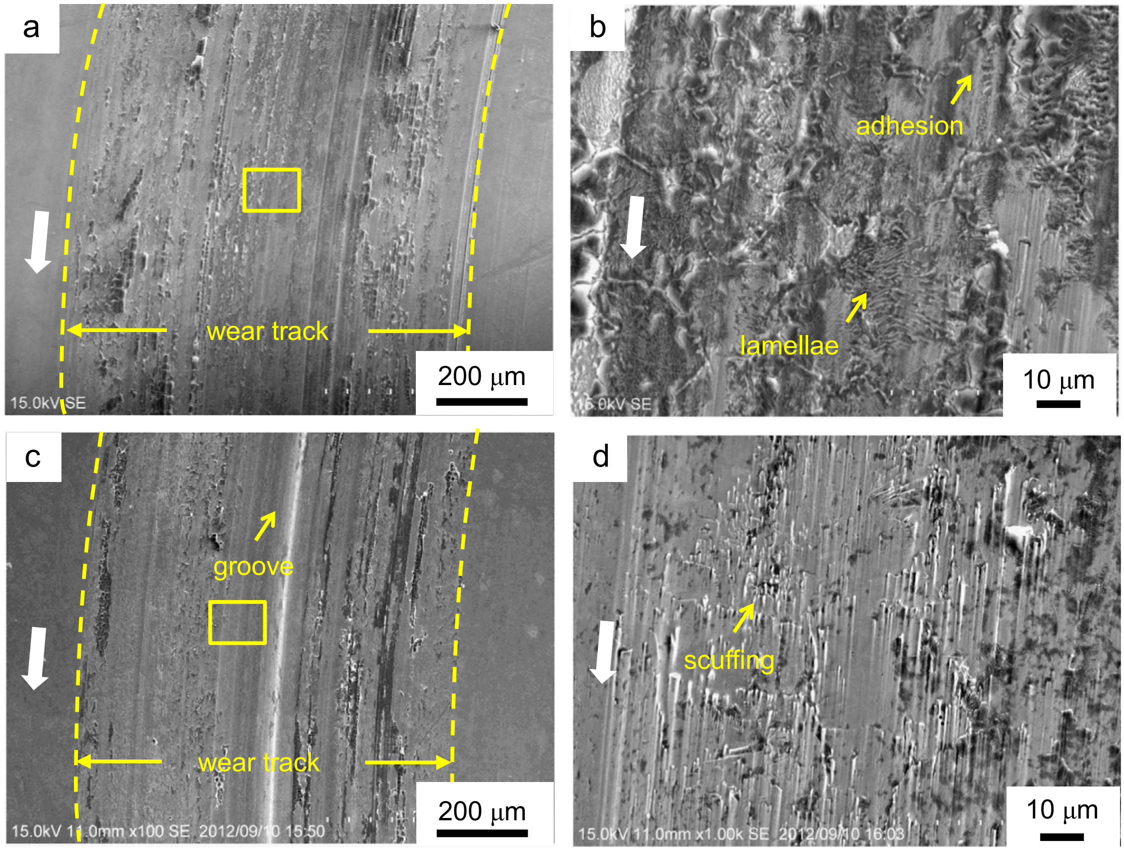

Fig. 9. The SEM micrographs of the wear tracks on (a)(b) HP and (c)(d) HPA discs, respectively, in which the sliding directions of the pins are indicated by white arrows.

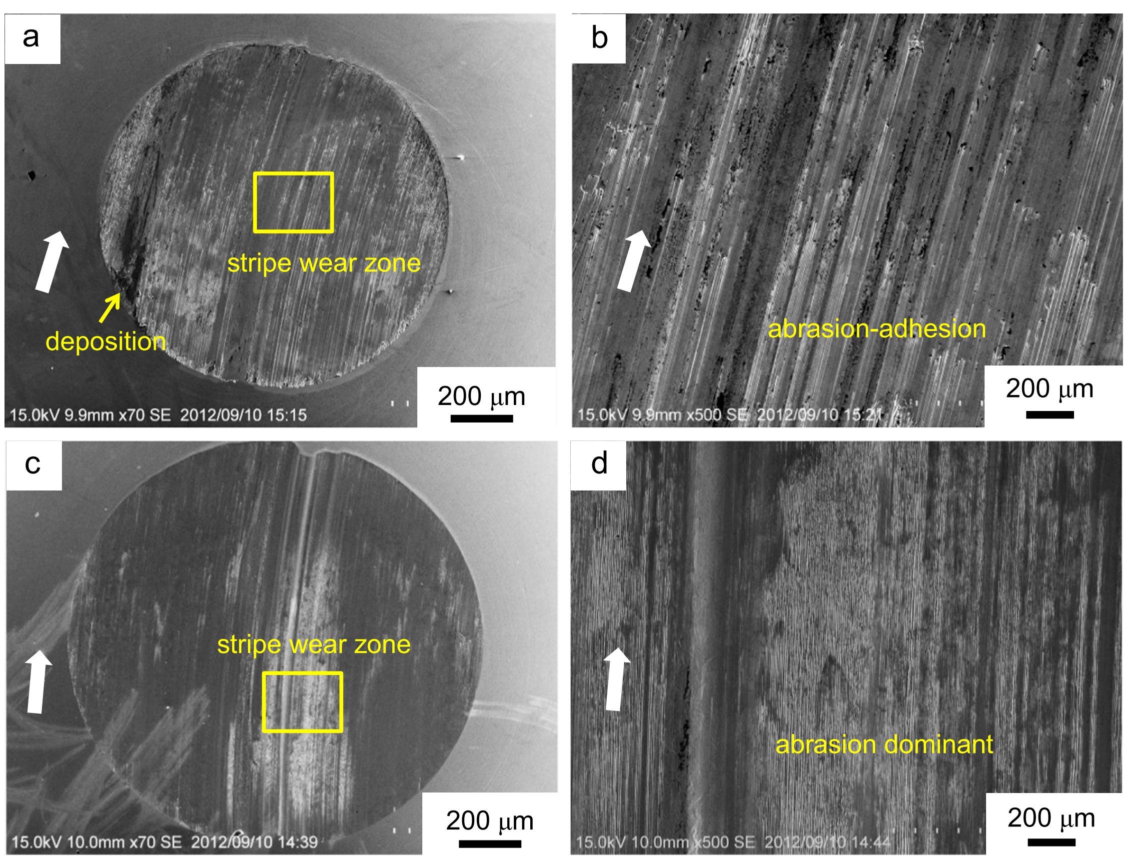

Fig. 10. The SEM micrographs of the worn topographies on (a) (b) HP and (c) (d) HPA pins, respectively, in which the sliding directions of the pins are indicated by white arrows.

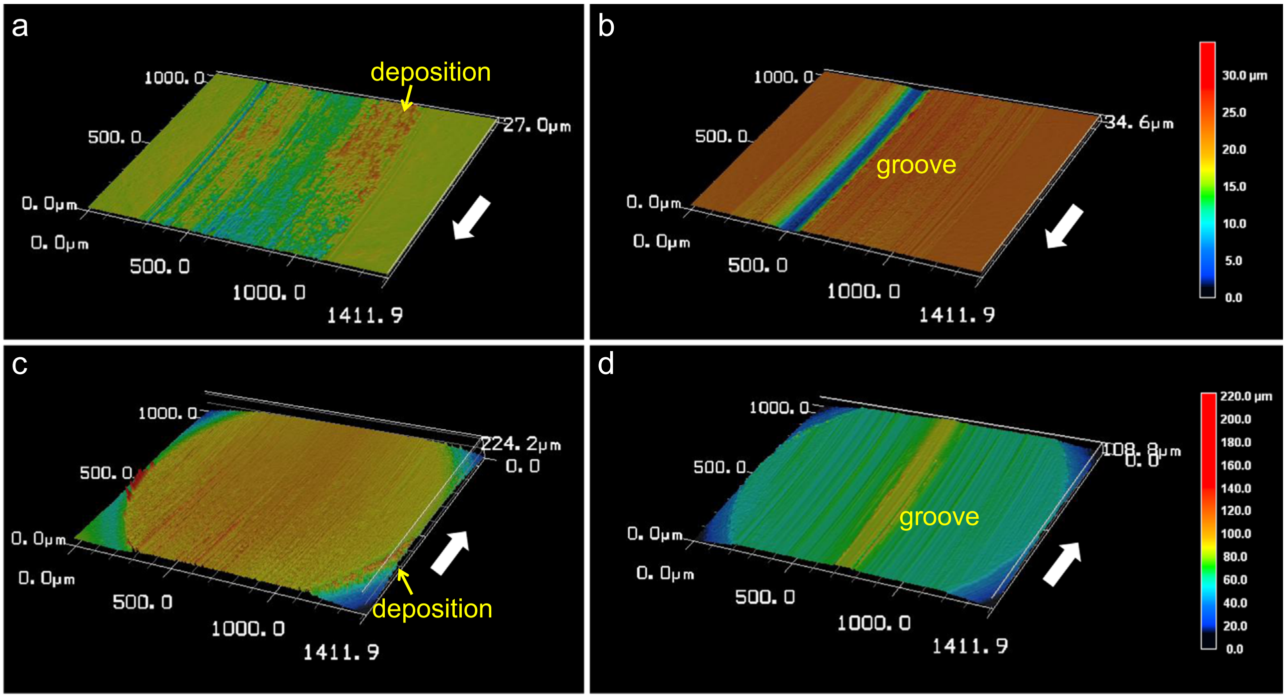

Fig. 11. The 3D micrographs of the worn surface topography on (a) HP, (b) HPA discs, and (c) HP, (d) HPA pins.

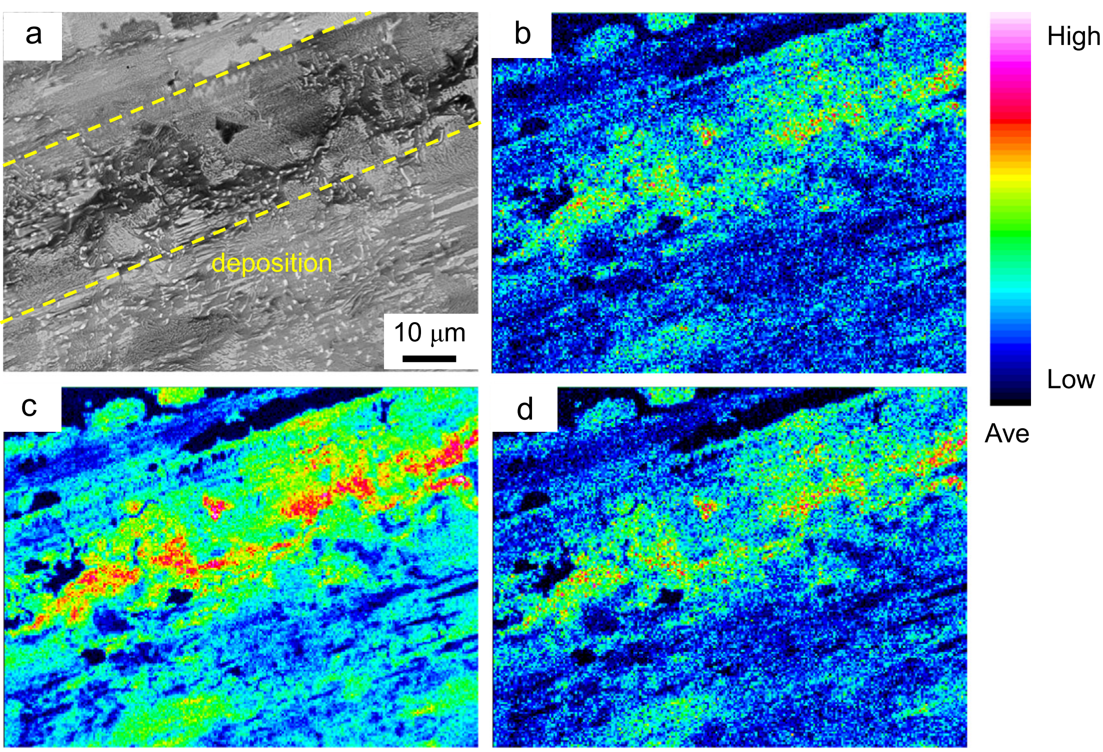

Fig. 12. Accumulation of tribochemical layer on the worn HP surface: (a) BSE image and X-ray mappings of (b) calcium, (c) oxygen and (d) phosphorous, suggesting that Ca-PO_4 compound was generated from tribochemical reactions during self-mating wear process.

tribochemical reactions during self-mating wear process, having some protect effect on the surfaces.

3.3. Micro hardness

The Vickers hardness before and after wear are shown in Fig. 13, in which general hardness of alloys were evaluated by HV1, and the hardness of individual phases by HV0.05 since small measuring load only produce a small area within individual grain (~ 40–50 μm) of resistance measured.

The results indicate that firstly, the HP has obvious higher hardness than HPA, judged by both HV1 and HV0.05. The higher value of micro hardness of as-polished HP is due to precipitate hardening and the ε-H.C.P. Co phases. On the one hand, the HP has more precipitates distributing in its matrix, as shown in Fig. 4; on the other hand, the ε-H.C.P. demonstrates higher hardness owing

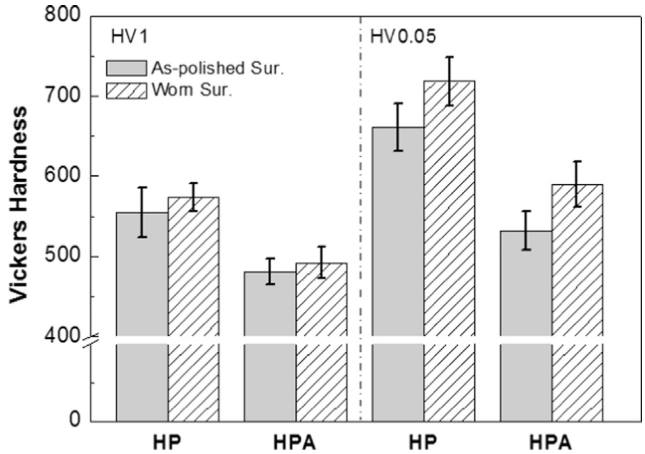

Fig. 13. Micro hardness, HV1 and HV0.05 of HP and HPA with their error bars (standard deviation, 10 measurements), indicating an increase of hardness after wear test.

to its limited slip systems compared to the γ-F.C.C Co phases [1,28,29].

Secondly, the standard deviations of HV0.05 are larger than that of HV1 for both HP and HPA, because grains with various precipitates exist in the matrix would have different responses to load applied. With HP, the HV0.05 is correlated to the carbide/nitride content as these precipitates are harder than the matrix [30]. For HPA, since the precipitates distributed uniformly in the matrix, the increment between HV1 and HV0.05 increased more than that between HP.

After the wear test, similar hardness increases were found for both HP and HPA. The increment in HV0.05 is larger than that in HV1, indicating that the work hardening concentrated at limited regions beneath the surfaces.

3.4. Surface roughness

Table 2 lists the arithmetic average roughness (Ra) of the as-polished and worn surface on discs. Student's *t*-test (assuming unequal variances, two-tail $p<0.01$) reveals that Ra for HP and HPA were significantly different from each other, under both as-polished and worn conditions. HP shows much coarser surface topography as a result of distinct lamellae inclusions, which are protuberant and stretch out like fences from matrix. The fences are considered to have effect to segregate direct contact of rubbing surfaces and detached debris.

The cross-sectional wear track profiles obtained by LM (Fig. 14) were used to determine how the wear has occurred [31]. Despite of similar widths of ~1 mm, the wear profile exhibit different track morphologies for the HP and HPA. The HPA wear profile shows a distinct V bend type, which was considered as a result of penetration of pin on the relative soft γ-F.C.C. matrix. The harder HP wear profile was notably lower in worn depth with more noisy at laterals, which is identical with the results of less material loss and more deposition on the surface (Figs. 8 and 11).

Table 2
Surface roughness of as-polished and worn surface on discs of HP and HPA (Ra: arithmetic average roughness, six measurements).

Ra (nm)	HP	HPA
As-polished surf.	29.68 ± 2.32	11.35 ± 1.72
Worn surf.	132.25 ± 41.44	139.65 ± 58.45

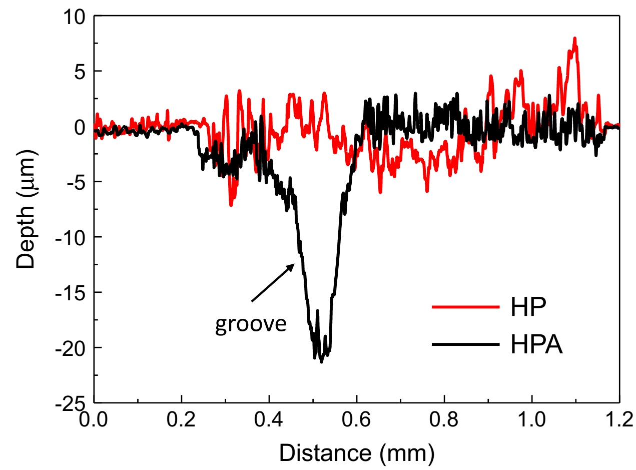

Fig. 14. The cross-sectional wear track profiles of HP and HPA after wear test.

4. Discussion

In this study, ε-H.C.P. HP with more lamellae precipitates was observed to have excellent wear resistance (low coefficient of friction and wear factor) compared to the γ-F.C.C. HPA. The results of average coefficients of friction and wear factors for metal-on-metal pin-on-disc pairings are tabulated in Table 3 along with published data for a comparison. It was observed that under similar saline-lubricated environment, the average stable coefficients of friction for CoCrMo alloys are between ~0.3 and 0.6 [3,17,32]. The common feature of the dynamic coefficients of friction was that it increases rapidly at initial contact, and then passes into a gradual increase, in which the latter phenomenon indicates stable contacts with prolonged sliding distances for all the pairings. High carbon cast alloys observed by Bedolla-Gil et al. demonstrate lower coefficients of friction, ~0.37, than that reported by Chiba et al., ~0.55, which is considered to be due to a relative shorter sliding distance (3.6 km) in the former tests than that in the latter (12.1 km). Generally, these stable coefficients of friction are comparable and consistent.

High carbon alloys of ASTM F75 [32], HC-wrought (high carbon wrought CoCrMo alloy) [17] and HPA were observed to demonstrate higher coefficients of friction, implying more tangential frictions and rougher contacts. A similarity for their surface topographies are the existence of inhomogeneous precipitates in the matrices. ASTM F75 demonstrates network of carbides along the grain boundaries; HC-wrought globular carbide segregation along rolling direction; and HPA an inhomogeneous lamellar carbide distribution in the grains. The inhomogeneous distribution of inclusions would lead to precipitate/precipitate contacts, where high contact stresses and frictional energy concentrate [33]; also they penetrate into soft matrix to generate plowing and groove on the surfaces. These alloys with inhomogeneous precipitates have longer run-in time to get steady, conforming wear between the mating surfaces.

Besides, forged low carbon alloys, in which few precipitates exist, were observed with medium coefficients of friction [13]. This may be due to the generation of dual-phase matrix during wear, which is considered to be responsible for the lower friction resistance of the alloys. The basic difference between LC-wrought (low carbon wrought CoCrMo alloy) [17] and forged LC CoCr alloy [32] to affect friction exists in nitride content, which would affect the consequent quantities of strain-induced martensite. We have estimated approximately that the $\gamma \rightarrow \varepsilon$ phase transformation were 17% and 75% for LC-wrought (0.14% N) and

Table 3
The average coefficient of friction (μ) and wear factor ($\times 10^{-7}$ mm^3/N m) for saline-lubricated MOM pin-on-disc wear tests with various CoCrMo alloys.

CoCrMo alloys			Topography and microstructure	Test parameters			Average CoF (m)	Wear factor ($\times 10^{-7}$ mm3/N m)		
				Initial contact pressure (GPa)	Lubricant	Sliding distance (km)		Pin	Disc	Total
Low carbon		Forged CoCr [26]	γ-F.C.C.	0.003	Hanks	12.1	0.59	7.6	12	19.6
		LC-wrought [14]	Globular σ,γ-F.C.C.	1.69	Hanks	12.1	0.39	5.81	21.25	27.06
High carbon	Cast	ASTM F75[26]	Interdendritic M23C6, γ-F.C.C.	0.003	Hanks	12.1	0.55	7.1	30	37.1
		As-cast [3]	Blocky+lamellar M23C6, γ-F.C.C.	1.96	Ringer	3.5	0.34	3.04	33.42	36.46
		1 h-sol [3]	Globular M23C6, γ-F.C.C.	1.96	Ringer	3.5	0.33	3.91	5.86	9.77
		6 h-sol [3]	Globular M23C6, γ-F.C.C.	1.96	Ringer	3.5	0.31	3.34	24.74	28.08
		8 h-aged [3]	Globular M23C6, 35 wt.% ε-H.C.P.	1.96	Ringer	3.5	0.45	6.55	3.08	9.63
		15 h-aged [3]	Globular M23C6, 60 wt.% ε-H.C.P.	1.96	Ringer	3.5	0.45	5.47	5.99	11.46
	Forged	HC-wrought [14]	Globular M23C6, γ-F.C.C.	1.69	Hanks	12.1	0.52	3.47	29.03	32.50
	Hot pressed	HP	Lamellae M23C6 and M2N, ε-H.C.P.	1.69	Hanks	12.1	0.33	4.19	8.44	12.63
		HPA	Lamellae M23C6, γ-F.C.C.	1.69	Hanks	12.1	0.52	4.66	20.79	25.45

Forged CoCr alloys (0.001% N), respectively [34]. The strain-induced martensite tended to generate hard debris between surfaces [3], and the debris is hard to be compressed or deformed, to cause unstable and "noisy" coefficients of friction.

In contrast, 6h-sol [3] and HP exhibit excellent friction resistance as a result of extremely low coefficients of friction. Despite of their disparate microstructures (for example, 6h-sol: few globular carbide in γ-F.C.C. matrix, whereas HP: plenty of lamellar precipitates in ε-H.C.P. matrix), a common point found for the both alloys was homogeneous microstructures. For 6h-sol, tiny globular carbides were observed dispersing homogeneously in γ-F.C.C. matrix (similar to the microstructure of As-cast and 1h sol [3]); for HP, coarse and fine lamellar precipitates bestrewing homogeneously ε-H.C.P. matrix. In contrast, other alloys with inhomogeneous microstructure were observed to have higher coefficients of friction. Hence we conclude that surface topography is considered to be more significant to affect coefficient of friction and friction than the microstructure itself.

The wear factors ($\times 10^{-7}$ mm^3/N m) for these saline-lubricated MOM pairings were also listed in Table 3 for comparison and analysis. It should be noticed that the initial pressures of these pairings are quite different for the Forged CoCr and ASTM F75 and other pairings. The former pairings, Forged CoCr and ASTM F75, with flat-ended pins, endure mild initial contact pressure of ~3 MPa; whereas for other pairings, on which severe initial contact pressures were ~2 GPa.

Most high carbon pairings (except for 8h-aged) show a trend that pins have less wear factors than discs, which is particularly obvious for the pairings with total wear factor larger than 25×10^{-7} mm^3/N m under harsh initial contact condition. We found that for As-cast, HC-wrought and 6h-sol, the wear factor differences between pin and disc were particularly evident, despite the various processing methods and microstructures. Although more investigation should be developed to make clear for the reason for the asymmetric wear, one conclusion can be conformed that these combinations should be restrained for the like-like pairings to prevent early invalidation.

Also we found that the wear factors are strongly affected by the matrix of the pairings.

According to the total wear factor, we divided these alloys into two groups: single γ-F.C.C. alloys (Forged CoCr, LC-wrought, ASTM F75, As-cast, 1h-sol, 6h-sol, HC-wrought and HPA) and partial or whole ε-H.C.P. alloys (8h-aged, 15-aged and HP), for a convenient analysis in this study.

The pairings (except for 1h-sol) in the single γ-F.C.C. group exhibit distinct higher total wear factors. Firstly, the as-cast materials, including ASTM F75 and as-cast, exhibit most losses as a result of coarse grains and similar interdendritic carbides along or inside grain boundaries. Secondly, high carbon alloys, despite of their process methods or microstructures, exhibit more wear losses than low carbon alloys. Hard carbides were introduced in the matrix for an anticipated enhancing effect of wear resistance; however, they are also responsible for the two-body wear while they penetrate into the relative soft γ-F.C.C. matrix; or then give rise to three-body wear and distinct pitting, while they are broken or torn-off at harsh contact.

It is noticeable that, for pairings made by the alloys with few precipitates in the original microstructures, i.e., Forged CoCr, wrought LC and 6h-sol, the wear factors are relatively moderate than that of other bearings in the same group as their matrix experienced phase transitions during wear. Although strain-induced martensite (SIM), as mentioned before, has been verified to have some adverse effect to increase coefficient of friction, it was also observed in Table 3 that Forged CoCr with distinct increase in SIM on worn surface shows less wear factor than that of LC-wrought and 6h-sol. It is interesting to find that LC-wrought with much higher initial contact pressure experienced relative less

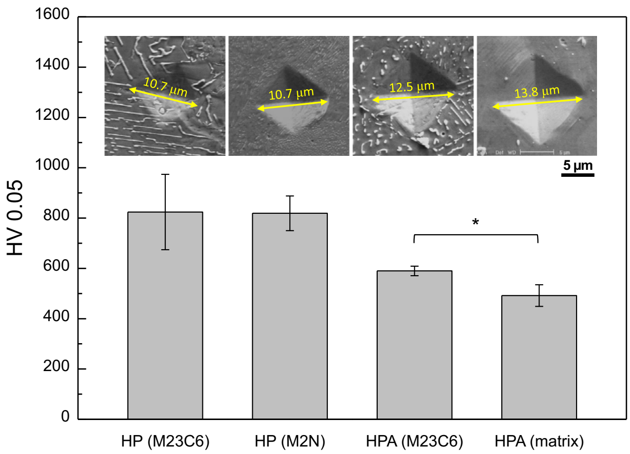

Fig. 15. Hardness of HP and HPA with various microstructures.

SIM, since the stacking fault energy is decreased and the γ-F.C.C. is much stabilized by nitrogen addition [19,20].

Similarly, the pairings in the ε-H.C.P. included group exhibit much lower total wear factors. Generally, ε-H.C.P. phase is much harder than γ-F.C.C phase due to its crystalline structure. The aged alloys, 8h-aged and 15-aged, possessing HV of ~350-370 [35], exhibit highest wear resistance compared with the as-cast or solute alloys. Also HP alloy with HV of ~550 exhibits dramatically low wear factor than other alloys under identified experimental conditions. The difference between aged cast alloys and hot pressed alloys may come from the different experiment parameters, such as lubricant, disc rotating speed, sliding distance, temperature, etc. However, high hardness of ε-H.C.P. phase could lower the depth of the track on the matrix and thus reduce abrasive wear of the CoCrMo alloys [36].

Since it has been mentioned (Fig. 13) that both HV1 and HV0.05 of HP is higher than that of HPA, it was also observed that, the distribution of precipitates is not homogenous for their separate grains. For HP, platelet-like lamellar carbides precipitate in some grains, while characteristic acicular lamellar nitrides in the other. For HPA, the acicular lamellar nitrides dissolved during annealing treatment (reverse transformation), leaving some grains with few precipitates, i.e., the grains with a similar microstructure to the matrix. The precipitates of $M_{23}C_6$ and M_2N, whose hardness are ~12 and 15 GPa [36-37], respectively, are expected to increase the hardness and wear resistance of the CoCrMo alloys. HV0.05 on grains with different microstructures were measured as shown in Fig. 15. Despite that the precipitates have different topographies (average size and spacing) and hardness, no significant difference was observed for the HV0.05 of HP grains with $M_{23}C_6$ or M_2N. However, the average hardness measured on the HPA grains with precipitates is obviously higher than that on the grains without precipitates. It could be speculated that the hardening effect of ε-H.C.P. HP is dominantly influenced by ε-phase whereas that of γ-F.C.C HPA is by the precipitates. As we have mentioned that the ε-H.C.P. phase has fewer slip systems and limited dislocation movement, consequently the HP exhibits superior wear resistance.

Lamellar precipitates, however, were also considered as one of the most significant factors for abrasion inhibition for HP bearings, since no obvious scuffing of micro-plowing or micro-cutting were observed on the worn surfaces. Similar stand-out effect of lamellar inclusion in steels was also reported by Moore et al, indicating that lamellar inclusions provide rigid barriers to plastic deformation and abrasion [38,39]. We noticed that two-body wear can dislodge the globular carbide by gradual removal of the surrounding matrix, then lead to the precipitate-torn-off pitting [3,17,40]. In contrast, lamellar precipitates are strongly embedded in the matrix to prevent pitting caused by the cyclic surface fatigue. However, for γ-F.C.C.HPA, lamellar carbides also affect as two-body abrasive wear on the counterbody of grains without precipitates since the γ-F.C.C. is weaker. Therefore, hard precipitates distributing homogeneously in the hard matrix (ε-H.C.P.) are considered to be one of the most significant factors to contribute wear resistance.

Finally, as common index for wear behavior evaluation, it was confirmed from the foregoing results that coefficients of friction have no direct relation with wear behaviors. coefficients of friction would be more affected by precipitate distribution and phase transformation, whereas wear behaviors, by matrix phase, i.e., hardness of the matrix, especially with homogeneous precipitation strengthening.

5. Conclusion

In the present study, the influence of the microstructure factors on the sliding behaviors of the high-carbon (HC) HP and HPA alloys were investigated to reach the following conclusions:

(1) Surface topography and precipitate distribution are more significant to affect friction performance than the microstructure itself, and HP with homogeneous precipitate distribution exhibits smooth, lower coefficient of friction;
(2) Sliding wear with more Ca-PO4 compound deposition is the dominant wear mechanism for HP; whereas abrasive wear with obvious plastic deformation for HPA;
(3) The wear rate of HPA was two times higher than that of HP. The higher hardness of HP is dominantly influenced by ε-H.C.P. matrix and can reduce the plastic abrasion;
(4) Lamellar carbides embedded unequally in γ-F.C.C.HPA accelerate two-body abrasive wear, whereas homogeneous lamellar precipitates in ε-H.C.P. HP can work as rigid barriers to prevent plastic deformation and abrasive wear;
(5) It may be suggested that hot-pressed CoCrMo alloys can be considered as a simple alternative wear-resistant material.

However, it is necessary to evaluate the friction and wear behavior of these alloys in physiological solutions, together with the presence of proteins and bio-organisms, by conducting both pin-on-disc and hip joint simulator wear tests for a potential biomedical application of hip joint prosthesis. Also the long-term biocompatibility related to the influence of the wear particles and metal ions should be concerned in our future work.

Acknowledgments

This research was mainly supported by a Regional Innovation Cluster Program 2010 from the Ministry of Education, Culture, Sports, Science and Technology of Japan. The authors would also like to express their appreciation to Mr. S. Ito and Mr. Y. Narita for their contribution to the work.

References

[1] W. Betterridge, Cobalt and its Alloys, Halsted Press, Chichester, 1982.
[2] J.C. Walker, R.B. Cook, J.W. Murray, A.T. Clare, Pulsed electron beam surface melting of CoCrMo alloy for biomedical applications, Wear 301 (2013) 250–256.
[3] Y. Bedolla-Gil, M.A.L. Hernandez-Rodriguez, Tribological behavior of a heat-treated Cobalt-based alloy, J. Mater. Eng. Perform 22 (2013) 541–547.
[4] J. Fisher, J.L. Tipper, M.H. Stone, C. Davies, P. Hatto, J. Bolton, M. Riley, C. Hardaker, G.H. Isaac, G. Berry, J. Mater, Wear of surface engineered metal-on-metal hip prostheses,, Sci.-Mater. Med. 15 (2004) 225–235.
[5] T.M. Devine, A. Wulff, Cast vs. wrought cobalt-chromium surgical implant alloys, J. Biomed. Mater. Res. 9 (1975) 151–167.

[6] H.S. Dobbs, J.L.M. Robertson, Heat treatment of cast Co-Cr-Mo for orthopaedic implant use, J. Mater. Sci. 18 (1983) 391–401.
[7] A. Marti, Cobalt-base alloys used in bone surgery, Injury 31 (2000) S-D18–S-D21.
[8] M.M. Dewidar, H. Yoon, J.K. Lim, Mechanical properties of metals for biomedical applications using powder metallurgy process: A review, Met. Mater. Int. 12 (2006) 193–206.
[9] B. Patel, G. Favaro, F. Inam, M.J. Reece, A. Angadji, W. Bonfield, J. Huang, M. Edirisinghe, Cobalt-based orthopaedic alloys: Relationship between forming route, microstructure and tribological performance, Mater. Sci. Eng C 32 (2012) 1222–1229.
[10] M. Semlitsch, H.G. Willert, Properties of implant alloys for artificial hip joints, Med. Biol. Eng. Comput. 18 (1980) 511–552.
[11] M. Niinomi, Recent metallic materials for biomedical applications, Metall. Mater. Trans. A 33 (2002) 477–486.
[12] Z. Doni, A.C. Alves, F. Toptan, J.R. Gomes, A. Ramalho, M. Buciumeanu, L. Palaghian, F.S. Silva, Dry sliding and tribocorrosion behaviour of hot pressed CoCrMo biomedical alloy as compared with the cast CoCrMo and Ti6Al4V alloys, Mater. Design 52 (2013) 47–57.
[13] B. Henriques, D. Soares, F.S. Silva, Microstructure, hardness, corrosion resistance and porcelain shear bond strength comparison between cast and hot pressed CoCrMo alloy for metal–ceramic dental restorations, J. Mech. Beh. Biomed. Mater. 12 (2012) 83–92.
[14] J. Cawley, J. Metcalf, A. Jones, T. Band, D. Skupien, A tribological study of cobalt chromium molybdenum alloys used in metal-on-metal resurfacing hip arthroplasty, Wear 225 (2003) 999–1006.
[15] D. Dowson, C. Hardaker, M. Flett, G. Issac, A hip joint simulator study of the performance of metal-on-metal joints, J. Arthroplasty 19 (2004) 118–123.
[16] M. Hernandez, R. Mercado, A. Perez, D. Martinez, M. Cantu, Wear of cast metal-metal pairs for total replacement hip prostheses, Wear 259 (2005) 958–963.
[17] Y. Chen, Y. Li, S. Kurosu, K. Yamanaka, N. Tang, Y. Koizumi, A. Chiba, Effects of sigma phase and carbide on the wear behavior of CoCrMo alloys in Hanks' solution, Wear 310 (2014) 51–62.
[18] K. Yamanaka, M. Mori, A. Chiba, Nanoarchitectured Co–Cr–Mo orthopedic implant alloys: Nitrogen-enhanced nanostructural evolution and its effect on phase stability, Acta Biomater. 9 (2013) 6259–6267.
[19] Y. Li, Y. Yamashita, N. Tang, B. Liu, S. Kurosu, H. Matsumoto, Y. Koizumi, A. Chiba,Influence, of carbon and nitrogen addition on microstructure and hot deformation behavior of biomedical Co-Cr-Mo alloy, Mater. Chem. Phys. 135 (2012) 849–854.
[20] Y. Li, J. Yu, S. Kurosu, Y. Koizumi, H. Matsumoto, A. Chiba, Role of nitrogen addition in stabilizing the γ phase of Co-29Cr-6Mo alloy, Mater. Chem. Phys 133 (2012) 29–32.
[21] S. Kurosu, H. Matsumoto, A. Chiba, Grain refinement of biomedical Co-27Cr-5Mo-0.16N alloy by reverse transformation, Mater. Lett. 64 (2010) 49–52.
[22] H.R. Hertz, Über die Berührung fester elastischer Körper und über die Härte, Sitzungsbericht des Vereins zur Förderung des Gewerbefleiβes (1882) 449–463.
[23] J. Fisher, D. Dowson, Tribology of total artificial joints, Proc. Inst. Mech. Eng. H 205 (1991) 73–79.
[24] ASTM E92, Standard Test Method for Vickers Hardness of Metallic Materials, ASTM International, West Conshohocken, PA (2003).
[25] S. Das Bakshi, P.H. Shipway, H.K.D.H. Bhadeshia, Three-body abrasive wear of fine pearlite, nanostructured bainite and martensite, Wear 308 (2013) 46–53.
[26] B. Patel, G. Favaro, F. Inam, M.J. Reece, A. Angadji, W. Bonfield, J. Huang, M. Edirisinghe, Cobalt-based orthopaedic alloys: Relationship between forming route, microstructure and tribological performance, Mater. Sci. Eng. C 32 (2012) 1222–1229.
[27] S. Mischler, A.I. Muñoz, Wear of CoCrMo alloys used in metal-on-metal hip joints: A tribocorrosion appraisal, Wear 297 (2013) 1081–1094.
[28] Wear of Metals, in: D.H. Buckley, A.D. Sarker (Eds.), Pergamon Press, New York, 1976, pp. 93–95.
[29] B.D. Ratner, A.S. Hoffman, J.S. Frederick, E.L. Jack, Biomaterials Science: An Introduction to Materials in Medicine, Academic Press, Oxford, 2004.
[30] M. Dourandish, D. Godlinski, A. Simchi, V. Firouzdor, Sintering of biocompatible P/M Co–Cr–Mo alloy (F-75) for fabrication of porosity-graded composite structures, Mater. Sci. Eng. A 472 (2008) 338–346.
[31] B. Patel, G. Favaro, F. Inam, M.J. Reece, A. Angadji, W. Bonfield, J. Huang, M. Edirisinghe, Cobalt-based orthopaedic alloys: Relationship between forming route, microstructure and tribological performance, Mater. Sci. Eng C 32 (2012) 1222–1229.
[32] A. Chiba, K. Kumagai, N. Nomura, S. Miyakawa, Pin on disk wear behavior in a like-on-like configuration in a biological environment of high carbon cast and low carbon forged Co-29Cr-6Mo alloys, Acta Mater. 55 (2007) 1309–1318.
[33] G.W. Stachowiak, A.W. Batchelor, Fundamentals of contact between solids, Elsevier Science Publishers B.V., 1993 (Tribology Series, 24, Engineer Tribology).
[34] M. Sage, C.h. Guillaud, Revue de Metallugie, Siderurgy Research Institute (I.R.S. I.D.), XLVII 2 (1950) 139–145.
[35] ⟨http://www.tribology-abc.com/calculators/hardness.htm⟩.
[36] H. Berns、G. Scheibelein、W. Theisen, Ferrous Materials: Steel and Cast Iron.
[37] The Japan Institute of Metals and Material. The Data Book for the Metals, third ed., Maruzen, Tokyo, 1993, pp. 159-163.
[38] M.A. Moore, The relationship between the abrasive wear resistance hardness and microstructure of ferritic materials, Wear 28 (1974) 59–68.
[39] K.-H. Zum Gahr, Wear by hard particles, Tribol. Int. 31 (1998) 587–596.
[40] M.A. Wimmer, J. Loos, R. Nassutt, M. Heitkemper, A. Fischer., The acting wear mechanisms on metal-on-metal hip joint bearings: In vitro results, Wear 250 (2001) 129–139.